Monthly Notices
of the
ROYAL ASTRONOMICAL SOCIETY

MNRAS **431,** 3685–3696 (2013)
Advance Access publication 2013 April 5

doi:10.1093/mnras/stt453

Spectrum analysis of bright *Kepler* late B- to early F-stars★

A. Tkachenko,[1]†‡ H. Lehmann,[2] B. Smalley[3] and K. Uytterhoeven[4,5]

[1]*Instituut voor Sterrenkunde, K.U. Leuven, Celestijnenlaan 200D, B-3001 Leuven, Belgium*
[2]*Thüringer Landessternwarte Tautenburg, D-07778 Tautenburg, Germany*
[3]*Astrophysics Group, Keele University, Staffordshire ST5 5BG, UK*
[4]*Instituto de Astrofísica de Canarias (IAC), Calle Via Lactea s/n, 38205 La Laguna, Tenerife, Spain*
[5]*Department Astrofísica, Universidad de La Laguna (ULL), Tenerife, Spain*

Accepted 2013 March 12. Received 2013 March 12; in original form 2012 November 18

ABSTRACT

The *Kepler* satellite mission was designed to search for transiting exoplanets and delivers single band-pass light curves of a huge number of stars observed in the Cygnus–Lyra region. At the same time, it opens a new window for asteroseismology. In order to accomplish one of the required preconditions for the asteroseismic modelling of the stars, namely knowledge of their precise fundamental parameters, ground-based spectroscopic and/or photometric follow-up observations are needed. We aim to derive fundamental parameters and individual abundances for a sample of 18 γ Dor/δ Sct and 8 slowly pulsating B (SPB)/β Cep candidate stars in the *Kepler* satellite field of view. We use the spectral synthesis method to model newly obtained, high-resolution spectra of 26 stars in order to derive their fundamental parameters like $T_{\rm eff}$, $\log g$, $v \sin i$, ξ, [M/H] and individual abundances with high accuracy. The stars are then placed into the $\log(T_{\rm eff}) - \log(g)$ diagram and the obtained spectroscopic classification is compared to the existing photometric one. For most A- and F-type stars, the derived $T_{\rm eff}$ values agree within the measurement errors with the values given in the *Kepler* Input Catalog (KIC). For hot stars, the KIC temperatures appear to be systematically underestimated, in agreement with previous findings. We also find that the temperatures derived from our spectra agree reasonably well with those derived from the spectral energy distribution fitting. According to their position in the $\log(T_{\rm eff}) - \log(g)$ diagram, two stars are expected γ Dor stars, four stars are expected δ Sct stars and four stars are possibly δ Sct stars at the blue edge of the instability strip. Two stars are confirmed SPB variables, and one star falls into the SPB instability region but its parameters might be biased by binarity. Two of the four stars that fall into the δ Sct instability region show γ Dor-type oscillation in their light curves implying that γ Dor-like oscillations are much more common among the δ Sct stars than what is theoretically expected. Moreover, one of the stars located at the hot border of the δ Sct instability strip is classified as δ Sct–γ Dor hybrid pulsator from its light-curve analysis. Given that these findings are fully consistent with recent investigations, we conclude that a revision of the γ Dor and δ Sct instability strips is essential.

Key words: stars: abundances – stars: fundamental parameters – stars: variables: δ Scuti.

1 INTRODUCTION

Though the primary goal of actual space missions like *Convection Rotation and Planetary Transits* (*CoRoT*; Auvergne et al. 2009) and *Kepler* (Gilliland et al. 2010) is to search for transiting exoplanet systems, the almost uninterrupted time series of high-quality data led to the discovery of a huge number of pulsating stars. This opened up a new era in asteroseismology, the study of stellar interiors via the interpretation of pulsation patterns observed at the surfaces of the stars.

The amount of data delivered by these space missions is huge implying the need in establishing methods of automatic classification of the stars. In the case of *Kepler* data, such methods are usually based on the (single band-pass) light-curve morphology and/or interpretation of the corresponding Fourier spectrum.

★Based on observations with the 2-m Alfred-Jensch-Telescope of the Thüringer Landessternwarte Tautenburg.

† Postdoctoral Fellow of the Fund for Scientific Research (FWO), Flanders, Belgium.
‡ E-mail: andrew@ster.kuleuven.be

Quite often, this leads to simultaneous assignment of the same object to different classes of variable stars. The photometric signal of e.g. an ellipsoidal variable can easily be misinterpreted by rotational modulation due to stellar surface inhomogeneities or by low-frequency stellar pulsations. Moreover, there are classes of pulsating stars like the Gamma Doradus and slowly pulsating B (SPB) stars showing the same type of variability in their light curves but residing at different locations in the Hertzsprung–Russell diagram. The way to discriminate between them is to derive their effective temperatures and log g. This is one reason why ground-based follow-up spectroscopic and/or multicolour photometric observations are essential (see the ground-based follow-up campaign for *Kepler* asteroseismic targets as described by Uytterhoeven et al. 2010a,b). Moreover, high-resolution, high-signal-to-noise (S/N) spectroscopic observations allow one to unreveal the nature of binary and rotationally modulated stars by observing systematic Doppler shifts of all lines in the spectrum or 'moving bumps' across the line profiles of certain chemical elements, respectively. The evaluated atmospheric parameters from ground-based data like effective temperature $T_{\rm eff}$, surface gravity log $g$and metallicity [M/H] can further be used for an in-depth asteroseismic modelling of stars in combination with high-quality photometric data gathered by the satellites.

In this paper, we focus on SPB/β Cep and γ Dor/δ Sct candidate stars in the *Kepler* field of view. The term 'slowly pulsating B stars' (SPB) was introduced by Waelkens (1991), who detected multiperiodic brightness and colour variations for seven stars with spectral types between B3 and B9. These stars have masses between 3 and 7 $M_{\odot}$. The observed photometric and radial velocity (RV) variations are interpreted in terms of low-degree l, high radial order n gravity mode pulsations characterized by intrinsic periods roughly between 0.8 and 3 d (e.g. De Cat et al. 2004; Aerts, Christensen-Dalsgaard & Kurtz 2010). The theoretical instability strip of SPBs overlaps with the instability region of β Cepheii (β Cep) pulsators, which have higher masses (between 8 and 18 $M_{\odot}$) and are typically hotter than SPB variables. β Cep stars pulsate in low radial order pressure (p-) and gravity (g-) modes with periods between 2 and 8 h (Aerts et al. 2010).

γ Dor and δ Sct-type stars are the two other classes of variable pulsating stars where the theoretical instability strips overlap. Similar to SPB stars, γ Dor stars pulsate in low-degree, high-order g-modes with periods between 0.5 and 3 d (Kaye et al. 1999). It is difficult to discriminate between γ Dor and SPB-type pulsators based on the light-curve morphology and Fourier spectrum only without having information about the temperature of the star. The observed variability of the δ Sct stars is understood in terms of low-order p-modes with periods between 18 min and 8 h (Aerts et al. 2010). The fact that γ Dor and δ Sct instability regions overlap suggests that *hybrid pulsators* showing both pulsation characteristics, i.e. high-order g-modes and lower order p- and g-modes, must exist.

In this paper, we present the results of the spectroscopic analysis of 8 SPB/β Cep and 18 γ Dor/δ Sct candidate stars in the *Kepler* field of view. After deriving the fundamental parameters of our sample stars, we classify them according to the expected type of variability and compare the results to the classification expected from the *Kepler* light-curve analysis. For every star in the sample, we additionally check the spectra for RV and line profile variation (LPV) to unreveal the possible binary nature of the star. The observational material and the data reduction procedure are described in Section 2. The method and the results of the spectrum analysis are presented in Sections 3 and 4, respectively. We discuss the results obtained for late B- to early A-type stars in Section 4.1 and for intermediate A- to early F-type stars in Section 4.2. In Section 6, we compare our derived fundamental parameters with the *Kepler* Input Catalog (KIC) values; the overall conclusions are presented in Section 7.

2 OBSERVATIONS

We base our analysis on high-resolution, high-S/N spectra taken with the Coudé-Echelle spectrograph attached to the 2-m telescope of the Thüringer Landessternwarte Tautenburg. The spectra have a resolution of 32 000 and cover the wavelength range from 4720 to 7400 Å. Table 1 represents the journal of observations and gives the KIC number, an alternative designation, the number of obtained spectra, the visual magnitude and the spectral type as indicated in the SIMBAD data base. The number of acquired spectra is different for different stars since we aimed to reach an S/N of about 100 for the mean, averaged spectrum of each object.

The data were reduced using standard European Southern Observatory MIDAS packages. The data reduction included bias and stray-light subtraction, cosmic rays filtering, flat fielding using a halogen lamp, wavelength calibration using a ThAr lamp and normalization to the local continuum. All spectra were additionally corrected in wavelength for individual instrumental shifts by using a large number of telluric O_2 lines. The cross-correlation technique was used to measure the RVs from the single spectra so that the single spectra finally could be shifted and co-added to build the mean, high-S/N averaged spectrum of each star.

We use publicly available both long- (time resolution ∼30 min) and short-cadence (time resolution ∼1 min) *Kepler* data to make an additional check for binarity, stellar activity and pulsations for each star in the sample. The *Kepler* data are released in quarters,

Table 1. Journal of observations. All spectra have been taken in 2011. N gives the number of acquired spectra, V the visual magnitude and SpT the spectral type as indicated in the SIMBAD data base.

KIC	Designation	N	V	SpT
02571868	HD 182271	3	8.7	A0
02859567	HD 184217	2	8.3	A0
02987660	HD 182634	3	8.0	A3
03629496	HD 177877	2	8.3	A0
04180199	HD 225718	9	10.1	–
04989900	HD 175841	2	6.9	A2
05356349	HD 181680	2	8.1	A0
05437206	HD 179936	1	8.4	A2
06668729	HD 175536	1	8.6	A2
07304385	TYC 3145-901-1	6	10.1	–
07827131	HD 184695	2	8.0	A2
07974841	TYC 3148-1470-1	2	8.2	–
08018827	HD 179817	2	8.1	B9
08324268	HD 189160	4	8.0	A0p
08351193	HD 177152	4	7.6	B9
08489712	HD 181598	2	8.6	A0
08915335	HD 190566	6	9.6	A2
09291618	BD +452961	6	9.7	A5
09351622	BD +452955	4	9.1	F0
10096499	HD 189013	2	6.9	A2
10537907	BD +472856	7	9.9	F0
10974032	HD 182828	2	8.4	A0
11572666	TYC 3565-1155-1	5	9.9	–
11874676	BD +493106	7	10.1	A5
12153021	HD 179617	3	8.7	A2
12217324	HD 186774	2	8.3	A0

i.e. periods between two spacecraft rolls. For this study, we use the data from quarters Q0–Q6 (2009 May–2010 September) where available.

3 METHOD

Our code GSSP (Tkachenko et al. 2012) finds the optimum values of $T_{\rm eff}$, $\log g$, ξ, [M/H] and $v \sin i$ from the minimum in χ^2 obtained from a comparison of the observed spectrum with the synthetic ones computed from all possible combinations of the above-mentioned parameters. The errors of measurement (1σ confidence level) are calculated from the χ^2 statistics using the projections of the hypersurface of the χ^2 from all grid points of all parameters on to the parameter in question. In this way, the estimated error bars include any possible model-inherent correlations between the parameters. Possible imperfection of the model-like incorrect atomic data, non-local thermodynamic equilibrium (non-LTE) effects or continuum normalization are not taken into account, of course. Fossati et al. (2007, 2008) state that the continuum normalization is a source of abundance uncertainty that can raise from about 0.1 to 0.2 dex for large $v \sin i$. We corrected the observed spectra during the analysis for large-scale imperfections of the continua by adjusting them to the model continua. The errors of the fit become a bit larger in this way, due to the inclusion of additional free parameters. Thus, we believe that the latter value mentioned by Fossati et al. (2007, 2008) is an upper limit given that the abundance uncertainty due to small-scale continuum imperfections should decrease with increasing number of analysed spectral lines.

In a recent study by Molenda-Żakowicz et al. (2013), the use of different methods and codes to derive atmospheric parameters for F, G, K and M-type stars is compared, and leads the authors to conclude that the realistic accuracy in the determination of atmospheric parameters for these types of stars is ± 150 K in $T_{\rm eff}$, ± 0.15 dex in [Fe/H] and 0.3 dex in $\log g$, even though error calculations for individual programs might result in smaller errors. Hence, we are aware of a possible underestimation of errors in Table 2.

In order to check how reliable our error estimates on elemental abundances are, we made an additional test represented in Fig. 1. We have chosen KIC 02571868, the star with a large value of $v \sin i$ of ∼200 km s^{-1}, as its broad and rather shallow lines should have a lower sensitivity to the elemental abundance changes than, e.g., the lines of the slowly rotating star KIC 12217324. We would thus expect error bars to be larger for the star with broad lines, at least for the chemical elements represented by sufficient number of

Table 2. Fundamental stellar parameters. The values labelled with 'K' are taken from the KIC and given for comparison. Metallicity values labelled with '(Fe)' refer to the derived Fe abundance.

KIC	$T_{\rm eff}^{\rm K}$(K)	$\log g^{\rm K}$	[M/H]$^{\rm K}$	$T_{\rm eff}$(K)	$\log g$	[M/H]	$v \sin i$ (km s^{-1})	ξ (km s^{-1})	SpT$^{\rm K}$	SpT
02571868	7930	3.56	−0.21	7880^{+70}_{-70}	$3.42^{+0.13}_{-0.13}$	$-0.22^{+0.12}_{-0.12}$	$205.0^{+12.0}_{-12.0}$	$2.80^{+0.40}_{-0.40}$	A6 IV-III	A6 IV-III
02859567	9418	4.15	−0.05	9970^{+340}_{-340}	$3.87^{+0.11}_{-0.11}$	$-0.57^{+0.20}_{-0.20}$	$200.0^{+25.0}_{-25.0}$	2.0	A0.5 V	B9.5 IV-V
02987660[a]	7305	3.59	−0.01	7525^{+75}_{-75}	$3.46^{+0.29}_{-0.29}$	$-0.27^{+0.14}_{-0.14}$	$140.0^{+10.0}_{-10.0}$	$2.95^{+0.40}_{-0.40}$	A9 IV-III	A8 IV-III
03629496	9796	4.50	+0.43	$11\,320^{+210}_{-210}$	$3.75^{+0.10}_{-0.10}$	$-0.43^{+0.20}_{-0.20}$	$160.0^{+19.0}_{-19.0}$	2.0	B9.5 V	B8.5 IV
04180199[b]	7220	3.91	−0.15	7390^{+80}_{-80}	$4.05^{+0.32}_{-0.32}$	$-0.56^{+0.23}_{-0.23}$	$180.0^{+27.0}_{-27.0}$	$0.95^{+0.75}_{-0.75}$	A9.5 IV-V	A9 IV-V
04989900	7900	3.51	−1.87	8400^{+150}_{-150}	$3.08^{+0.11}_{-0.11}$	$-0.23^{+0.22}_{-0.22}$	$191.0^{+15.0}_{-15.0}$	$2.33^{+0.65}_{-0.65}$	A6 IV-III	A4 III-II
05356349	8295	3.91	−0.06	8820^{+180}_{-180}	$3.51^{+0.11}_{-0.11}$	$-0.55^{+0.27}_{-0.27}$	$197.0^{+24.0}_{-24.0}$	$2.06^{+0.74}_{-0.74}$	A5 IV-V	A2.5 IV-III
05437206	7710	3.67	−0.03	7870^{+100}_{-100}	$3.10^{+0.13}_{-0.13}$	$-0.24^{+0.14}_{-0.14}$	$125.5^{+7.5}_{-7.5}$	$2.75^{+0.45}_{-0.45}$	A7 IV	A6 III
06668729	7770	3.49	−0.16	7800^{+75}_{-75}	$3.49^{+0.25}_{-0.25}$	$-0.45^{+0.15}_{-0.15}$	$128.0^{+9.0}_{-9.0}$	$2.33^{+0.45}_{-0.45}$	A6.5 IV-III	A6.5 IV-III
07304385[a]	6890	3.60	−0.06	7020^{+70}_{-70}	$3.65^{+0.25}_{-0.25}$	$-0.32^{+0.10}_{-0.10}$	$64.5^{+2.8}_{-2.8}$	$2.45^{+0.25}_{-0.25}$	F2 IV	F1 IV
07827131	8285	3.49	−0.19	8015^{+120}_{-120}	$2.79^{+0.10}_{-0.10}$	−1.15(Fe)	$228.0^{+26.0}_{-26.0}$	$4.85^{+0.85}_{-0.85}$	A4.5 IV-III	A6 II-III
07974841	8930	3.82	−0.15	$10\,650^{+285}_{-285}$	$3.87^{+0.14}_{-0.14}$	$+0.00^{+0.13}_{-0.13}$	$33.0^{+5.0}_{-5.0}$	2.0	A2 IV-V	B9 IV-V
08018827	9188	3.65	−0.14	$10\,945^{+350}_{-350}$	$3.98^{+0.16}_{-0.16}$	$-0.44^{+0.25}_{-0.25}$	$243.0^{+32.0}_{-32.0}$	2.0	A1.5 IV-III	B8.5 V-IV
08324268[a]	9045	4.32	+0.27	$11\,370^{+440}_{-440}$	$3.35^{+0.20}_{-0.20}$	$+0.65^{+0.13}_{-0.13}$	$31.0^{+4.0}_{-4.0}$	2.0	A1.5 V	B8.5 III
08351193	8467	3.99	−0.14	9980^{+250}_{-250}	$3.80^{+0.15}_{-0.15}$	−2.35(Fe)	$180.0^{+29.0}_{-29.0}$	2.0	A4 IV-V	A0 IV-V
08489712	8350	3.52	−0.33	8270^{+150}_{-150}	$2.90^{+0.15}_{-0.15}$	$-0.60^{+0.25}_{-0.25}$	$119.0^{+14.0}_{-14.0}$	$1.25^{+0.70}_{-0.70}$	A4 IV-III	A4.5 III-II
08915335	7770	3.48	−0.13	8000^{+100}_{-100}	$3.15^{+0.11}_{-0.11}$	$-0.10^{+0.20}_{-0.20}$	$200.0^{+17.0}_{-17.0}$	$1.58^{+0.40}_{-0.40}$	A6.5 IV-III	A5.5 III
09291618	7610	3.61	−0.08	7530^{+75}_{-75}	$3.56^{+0.40}_{-0.40}$	$-0.36^{+0.20}_{-0.20}$	$177.0^{+18.0}_{-18.0}$	$1.10^{+0.60}_{-0.60}$	A7.5 IV-III	A8 IV-III
09351622[a]	7450	3.53	−0.22	7515^{+70}_{-70}	$3.17^{+0.30}_{-0.30}$	$-0.24^{+0.12}_{-0.12}$	$78.0^{+4.5}_{-4.5}$	$2.90^{+0.35}_{-0.35}$	A8 IV-III	A7.5 III
10096499	7780	4.13	−0.02	7960^{+85}_{-85}	$3.27^{+0.12}_{-0.12}$	$-0.60^{+0.13}_{-0.13}$	$89.5^{+5.5}_{-5.5}$	$2.78^{+0.40}_{-0.40}$	A7 V-IV	A5.5 III-IV
10537907[a]	7500	3.45	−0.27	7400^{+70}_{-70}	$3.51^{+0.30}_{-0.30}$	$-0.45^{+0.14}_{-0.14}$	$112.0^{+8.0}_{-8.0}$	$2.80^{+0.40}_{-0.40}$	A8 IV-III	A8.5 IV-III
10974032	9038	3.70	−0.33	9750^{+370}_{-370}	$3.75^{+0.20}_{-0.20}$	−0.80(Fe)	$270.0^{+32.0}_{-32.0}$	2.0	A2 IV	A0 IV
11572666[b]	7040	3.49	−0.62	7265^{+85}_{-85}	$4.10^{+0.45}_{-0.45}$	−1.00(Fe)	$180.5^{+31.0}_{-31.0}$	$1.90^{+0.85}_{-0.85}$	F1 IV-III	A9.5 V-IV
11874676[b]	8220	4.00	−0.14	7885^{+80}_{-80}	$3.57^{+0.25}_{-0.25}$	−1.00(Fe)	$203.5^{+27.0}_{-27.0}$	$2.97^{+0.75}_{-0.75}$	A5 IV-V	A6 IV-III
12153021	9041	3.90	−0.11	9010^{+80}_{-80}	$3.50^{+0.10}_{-0.10}$	$-0.05^{+0.15}_{-0.15}$	$18.0^{+2.7}_{-2.7}$	$2.02^{+0.65}_{-0.65}$	A2 IV-V	A2 IV-III
12217324	10 434	3.93	−0.09	$10\,380^{+270}_{-270}$	$3.75^{+0.15}_{-0.15}$	$+0.22^{+0.14}_{-0.14}$	$19.0^{+3.5}_{-3.5}$	2.0	B9 V-IV	B9.5 IV

[a]LPV detected; [b]Stars with composite spectra.

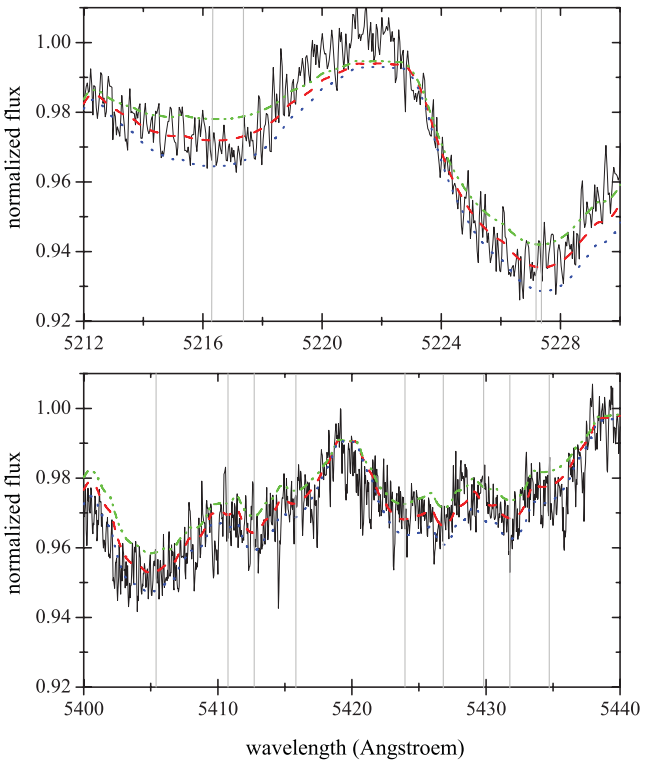

Figure 1. Fit of a part of the observed spectrum of KIC 02571868 (black, solid line) by synthetic spectra computed from our optimized parameters (red, dashed line) and assuming Fe abundance to vary within the quoted error bars of ±0.15 dex (blue, dotted and green, dash–dot-dotted lines, respectively). The vertical light grey lines indicate positions of (strongest) Fe lines.

individual lines in the stellar spectrum (e.g. Fe). Fig. 1 compares a part of the observed spectrum of KIC 02571868 with synthetic spectra computed assuming different Fe abundance that varies within the quoted error bars of ±0.15 dex (see Table 3). These rather small changes in Fe abundance cause quite clear deviations in the synthetic spectra and hence the difference in the quality of the fit. The corresponding values of χ^2 deviate from the optimal fit value by slightly more than the 1σ confidence level which is assumed to represent the errors of measurement as described above. The fact that the abundances of elements like Ti, Ca, etc. are derived for the slowly rotating star KIC 12217324 with lower precision than they are actually for the fast rotator KIC 02571868 is due to significant difference in atmospheric parameters, and temperature in particular. The above-mentioned elements are represented by a few, rather weak lines in the spectrum of KIC 12217324, which obviously makes the estimation of their abundances more challenging in this case and facilitates an increase of the corresponding error bars.

A detailed description of the method and its application to the spectra of *Kepler* β Cep and SPB candidate stars as well as δ Sct and γ Dor candidate stars are given in Lehmann et al. (2011) and Tkachenko et al. (2012), respectively.

For the calculation of synthetic spectra, we use the LTE-based code SYNTHV (Tsymbal 1996) which allows us to compute the spectra based on individual elemental abundances. The code uses precalculated atmosphere models which have been computed with the most recent, parallelized version of the LLMODELS program (Shulyak et al. 2004). Both programs make use of the Vienna Atomic Lines Database (Kupka et al. 2000) for a pre-selection of atomic spectral lines. The main limitation of the LLMODELS code is that the it is well suitable for early and intermediate spectral type stars but not for very hot and cool stars where non-LTE effects or absorption in molecular bands may become relevant, respectively.

4 RESULTS

Table 2 summarizes the results of the spectrum analysis for all stars of our sample. The first four columns of the table represent correspondingly the KIC number of the star, effective temperature $T_{\rm eff}^{\rm K}$, surface gravity $\log g^{\rm K}$ and metallicity $[{\rm M/H}]^{\rm K}$ as indicated in the KIC. The five following columns list the stellar parameters derived from our spectra, while the last two columns represent the spectral types as estimated from $T_{\rm eff}$ and $\log g$ given in the KIC and determined in this work, respectively. In both cases, the spectral types and the luminosity classes have been derived using an interpolation in the tables published by Schmidt-Kaler (1982). Metallicity values labelled with '(Fe)' refer to the derived Fe abundance; the corresponding measurement errors are given in Table 3. For the eight hottest stars of the sample (late B- to early A-type stars), the microturbulent velocity was fixed to a standard value of 2 km s^{-1} because of the strong correlation between ξ and $T_{\rm eff}$ for higher temperatures (see fig. 2 in Lehmann et al. 2011). In practice, this means that the errors in ξ raise up to about 1.5 km s^{-1} for stars with $T_{\rm eff} > 10\,000$ K and to about 3–4 km s^{-1} for stars hotter than 15 000 K. The results thus appear to be almost insensitive to the microturbulent velocity in this case.

Table 3 lists the elemental abundances derived for each target star. The metallicity given in the second column of the table refers to the initially derived chemical composition and was used as an initial guess for the determination of the individual abundances. The latter are given relative to solar values, i.e. negative/positive values refer to an under-/overabundance of the corresponding element compared to the solar composition. We assume the chemical composition of the Sun given by Grevesse, Asplund & Sauval (2007); corresponding values are listed in the header of Table 3 below the element designation. For five stars we have reached the lower metallicity limit of −0.8 dex in our grid of atmosphere models (KIC 07827131, 08351193, 10974032, 11572666 and 11874676) and give the derived Fe abundance instead. In all other cases, the derived Fe abundance matches the derived metallicity within the quoted error bars.

Similar to the results reported in two of our previous papers (Lehmann et al. 2011; Tkachenko et al. 2012), we find that the temperatures listed in the KIC are in general underestimated for the hotter stars. In the following, we discuss the results on individual stars in more detail.

4.1 Late B- to early A-type stars

Two of eight stars, KIC 08351193 and 10974032, are found to be metal poor with metallicities below the lower limit of −0.8 dex in our grid of atmosphere models. Both stars show nearly solar He abundance and overabundance of Mg compared to the derived Fe content, while the spectrum of KIC 08351193 additionally exhibits strong enhancement of Si. Both are fast rotators and hotter than what is expected from the KIC. The surface gravity is consistent with the one listed in the KIC in both cases. Balona et al. (2011) report the effective temperatures of 10 210 and 11 000 ± 400 K for KIC 08351193, determined from Strömgren photometry and from spectral energy distribution (SED) fitting to the combined SDSS,

Table 3. Metallicity and elemental abundances relative to solar ones in dex. Metallicity values labelled with '(Fe)' refer to the derived Fe abundance.

KIC	[M/H]	He −1.11	Fe −4.59	Mg −4.51	Si −4.53	Ti −7.14	Cr −6.40	O −3.38	Ca −5.73	Sc −8.99	Ni −5.81	C −3.65	Mn −6.65	Y −9.83
02571868	$-0.22^{+0.12}_{-0.12}$	–	$-0.25^{+0.15}_{-0.15}$	$-0.10^{+0.40}_{-0.40}$	$+0.20^{+0.35}_{-0.35}$	$-0.50^{+0.25}_{-0.25}$	$-0.05^{+0.20}_{-0.20}$	$-0.60^{+0.60}_{-0.60}$	$+0.00^{+0.20}_{-0.20}$	$-0.10^{+0.40}_{-0.40}$	$-0.45^{+0.30}_{-0.30}$	$-0.15^{+0.25}_{-0.25}$	$-0.65^{+0.45}_{-0.45}$	$-0.15^{+0.40}_{-0.40}$
02859567	$-0.57^{+0.20}_{-0.20}$	$+0.07^{+0.20}_{-0.20}$	$-0.75^{+0.25}_{-0.25}$	$-0.15^{+0.35}_{-0.35}$	$-0.25^{+0.35}_{-0.35}$	–	–	–	–	–	–	–	–	–
02987660	$-0.27^{+0.14}_{-0.14}$	–	$-0.35^{+0.16}_{-0.16}$	$+0.20^{+0.31}_{-0.31}$	$+0.05^{+0.40}_{-0.40}$	$-0.30^{+0.26}_{-0.26}$	$-0.40^{+0.25}_{-0.25}$	–	$-0.35^{+0.31}_{-0.31}$	$-0.25^{+0.45}_{-0.45}$	$-0.20^{+0.26}_{-0.26}$	$-0.05^{+0.25}_{-0.25}$	$-0.05^{+0.34}_{-0.34}$	$-0.40^{+0.40}_{-0.40}$
03629496	$-0.43^{+0.20}_{-0.20}$	$-0.07^{+0.20}_{-0.20}$	$-0.55^{+0.25}_{-0.25}$	$-0.45^{+0.35}_{-0.35}$	$-0.05^{+0.35}_{-0.35}$	–	–	–	–	–	–	–	–	–
04180199	$-0.56^{+0.23}_{-0.23}$	–	$-0.75^{+0.25}_{-0.25}$	$-0.15^{+0.35}_{-0.35}$	$-0.20^{+0.75}_{-0.75}$	$-0.85^{+0.50}_{-0.50}$	$-0.50^{+0.50}_{-0.50}$	–	$-0.35^{+0.50}_{-0.50}$	$-0.55^{+0.60}_{-0.60}$	$-0.60^{+0.45}_{-0.45}$	$-0.20^{+0.60}_{-0.60}$	$-0.35^{+0.75}_{-0.75}$	–
04989900	$-0.23^{+0.22}_{-0.22}$	–	$-0.20^{+0.22}_{-0.22}$	$-0.15^{+0.40}_{-0.40}$	$+0.10^{+0.46}_{-0.46}$	$-0.50^{+0.35}_{-0.35}$	$-0.30^{+0.32}_{-0.32}$	$-0.10^{+0.36}_{-0.36}$	$-0.45^{+0.35}_{-0.35}$	$+0.10^{+0.55}_{-0.55}$	$-0.05^{+0.41}_{-0.41}$	$+0.00^{+0.32}_{-0.32}$	$-0.20^{+0.45}_{-0.45}$	–
05356349	$-0.55^{+0.27}_{-0.27}$	–	$-0.70^{+0.23}_{-0.23}$	$-0.05^{+0.42}_{-0.42}$	$-0.20^{+0.50}_{-0.50}$	$-1.15^{+0.41}_{-0.41}$	$-1.05^{+0.65}_{-0.65}$	$-0.40^{+0.65}_{-0.65}$	$-0.60^{+0.47}_{-0.47}$	–	–	$-0.70^{+0.66}_{-0.66}$	–	–
05437206	$-0.24^{+0.14}_{-0.14}$	–	$-0.20^{+0.17}_{-0.17}$	$+0.20^{+0.41}_{-0.41}$	$+0.10^{+0.57}_{-0.57}$	$-0.40^{+0.26}_{-0.26}$	$-0.15^{+0.27}_{-0.27}$	$-0.05^{+0.40}_{-0.40}$	$-0.25^{+0.31}_{-0.31}$	$-0.10^{+0.35}_{-0.35}$	$-0.20^{+0.26}_{-0.26}$	$-0.05^{+0.26}_{-0.26}$	$-0.45^{+0.42}_{-0.42}$	$-0.20^{+0.45}_{-0.45}$
06668729	$-0.45^{+0.15}_{-0.15}$	–	$-0.40^{+0.17}_{-0.17}$	$+0.00^{+0.41}_{-0.41}$	$-0.05^{+0.56}_{-0.56}$	$-0.80^{+0.40}_{-0.40}$	$-0.45^{+0.36}_{-0.36}$	$-0.25^{+0.65}_{-0.65}$	$-0.35^{+0.35}_{-0.35}$	$-0.40^{+0.45}_{-0.45}$	$-0.60^{+0.41}_{-0.41}$	$-0.20^{+0.35}_{-0.35}$	$-0.25^{+0.50}_{-0.50}$	$-0.40^{+0.50}_{-0.50}$
07304385	$-0.32^{+0.10}_{-0.10}$	–	$-0.30^{+0.12}_{-0.12}$	$-0.10^{+0.21}_{-0.21}$	$-0.15^{+0.30}_{-0.30}$	$-0.35^{+0.22}_{-0.22}$	$-0.25^{+0.22}_{-0.22}$	–	$-0.20^{+0.20}_{-0.20}$	$-0.25^{+0.30}_{-0.30}$	$-0.30^{+0.21}_{-0.21}$	$-0.10^{+0.25}_{-0.25}$	$-0.20^{+0.32}_{-0.32}$	$-0.30^{+0.35}_{-0.35}$
07827131	−1.15(Fe)	–	$-1.15^{+0.22}_{-0.22}$	-0.80$^{+0.31}_{-0.31}$	$-0.55^{+0.50}_{-0.50}$	$-1.85^{+0.75}_{-0.75}$	$-1.30^{+0.67}_{-0.67}$	–	$-1.00^{+0.50}_{-0.50}$	–	–	$-0.90^{+0.52}_{-0.52}$	–	–
07974841	$+0.00^{+0.13}_{-0.13}$	$-0.92^{+0.20}_{-0.20}$	$+0.10^{+0.20}_{-0.20}$	$-0.35^{+0.35}_{-0.35}$	$-0.05^{+0.35}_{-0.35}$	$+0.15^{+0.35}_{-0.35}$	$+0.35^{+0.35}_{-0.35}$	–	–	–	–	–	–	–
08018827	$-0.44^{+0.25}_{-0.25}$	$+0.06^{+0.20}_{-0.20}$	$-0.45^{+0.25}_{-0.25}$	$+0.55^{+0.35}_{-0.35}$	$-0.55^{+0.35}_{-0.35}$	–	–	–	–	–	–	–	–	–
08324268	$+0.65^{+0.13}_{-0.13}$	abundances are not evaluated												
08351193	−2.35(Fe)	$+0.05^{+0.20}_{-0.20}$	$-2.35^{+0.25}_{-0.25}$	$-1.40^{+0.35}_{-0.35}$	$-1.20^{+0.35}_{-0.35}$	–	–	–	–	–	–	–	–	–
08489712	$-0.60^{+0.25}_{-0.25}$	–	$-0.50^{+0.23}_{-0.23}$	$-0.30^{+0.47}_{-0.47}$	$+0.00^{+0.47}_{-0.47}$	$-0.90^{+0.42}_{-0.42}$	$-0.50^{+0.48}_{-0.48}$	–	$-0.60^{+0.45}_{-0.45}$	–	–	$-0.30^{+0.52}_{-0.52}$	–	–
08915335	$-0.10^{+0.20}_{-0.20}$	–	$-0.05^{+0.17}_{-0.17}$	$+0.35^{+0.40}_{-0.40}$	$+0.80^{+0.32}_{-0.32}$	$-0.40^{+0.40}_{-0.40}$	$+0.20^{+0.27}_{-0.27}$	$-0.30^{+0.65}_{-0.65}$	$+0.00^{+0.36}_{-0.36}$	$-0.35^{+0.55}_{-0.55}$	$-0.25^{+0.37}_{-0.37}$	$-0.20^{+0.42}_{-0.42}$	$-0.35^{+0.50}_{-0.50}$	–
09291618	$-0.36^{+0.20}_{-0.20}$	–	$-0.40^{+0.23}_{-0.23}$	$-0.35^{+0.52}_{-0.52}$	$+0.20^{+0.40}_{-0.40}$	$-0.70^{+0.45}_{-0.45}$	$-0.55^{+0.40}_{-0.40}$	–	$-0.60^{+0.52}_{-0.52}$	$-0.50^{+0.65}_{-0.65}$	$-0.30^{+0.42}_{-0.42}$	$-0.10^{+0.35}_{-0.35}$	$-0.05^{+0.65}_{-0.65}$	–
09351622	$-0.24^{+0.12}_{-0.12}$	–	$-0.25^{+0.15}_{-0.15}$	$+0.00^{+0.30}_{-0.30}$	$+0.00^{+0.30}_{-0.30}$	$-0.40^{+0.20}_{-0.20}$	$-0.15^{+0.20}_{-0.20}$	–	$-0.15^{+0.21}_{-0.21}$	$-0.10^{+0.30}_{-0.30}$	$-0.25^{+0.22}_{-0.22}$	$-0.15^{+0.25}_{-0.25}$	$-0.15^{+0.30}_{-0.30}$	$-0.30^{+0.35}_{-0.35}$
10096499	$-0.60^{+0.13}_{-0.13}$	–	$-0.60^{+0.15}_{-0.15}$	$-0.10^{+0.30}_{-0.30}$	$-0.30^{+0.38}_{-0.38}$	$-0.80^{+0.29}_{-0.29}$	$-0.55^{+0.35}_{-0.35}$	$-0.30^{+0.65}_{-0.65}$	$-0.45^{+0.30}_{-0.30}$	$-0.65^{+0.42}_{-0.42}$	$-0.55^{+0.35}_{-0.35}$	$-0.45^{+0.35}_{-0.35}$	$-0.70^{+0.51}_{-0.51}$	–
10537907	$-0.45^{+0.14}_{-0.14}$	–	$-0.60^{+0.20}_{-0.20}$	$-0.20^{+0.40}_{-0.40}$	$-0.20^{+0.50}_{-0.50}$	$-0.50^{+0.25}_{-0.25}$	$-0.35^{+0.25}_{-0.25}$	–	$-0.25^{+0.31}_{-0.31}$	$-0.40^{+0.50}_{-0.50}$	$-0.55^{+0.29}_{-0.29}$	$-0.15^{+0.35}_{-0.35}$	$-0.40^{+0.40}_{-0.40}$	–
10974032	−0.80(Fe)	$-0.04^{+0.20}_{-0.20}$	$-0.80^{+0.27}_{-0.27}$	$+0.15^{+0.38}_{-0.38}$	$-0.50^{+0.36}_{-0.36}$	–	–	–	–	–	–	–	–	–
11572666	−1.00(Fe)	–	$-1.00^{+0.25}_{-0.25}$	$-0.40^{+0.40}_{-0.40}$	$-0.10^{+0.57}_{-0.57}$	$-0.95^{+0.48}_{-0.48}$	$-1.00^{+0.48}_{-0.48}$	–	$-0.80^{+0.47}_{-0.47}$	$-1.30^{+0.65}_{-0.65}$	$-0.65^{+0.45}_{-0.45}$	$-0.25^{+0.45}_{-0.45}$	$-0.70^{+0.67}_{-0.67}$	–
11874676	−1.00(Fe)	–	$-1.00^{+0.25}_{-0.25}$	$-0.10^{+0.47}_{-0.47}$	$-0.05^{+0.48}_{-0.48}$	$-1.00^{+0.50}_{-0.50}$	$-1.20^{+0.50}_{-0.50}$	–	$-0.65^{+0.47}_{-0.47}$	$-1.00^{+0.67}_{-0.67}$	$-0.75^{+0.45}_{-0.45}$	$-0.55^{+0.65}_{-0.65}$	–	–
12153021	$-0.05^{+0.15}_{-0.15}$	$+0.00^{+0.20}_{-0.20}$	$-0.10^{+0.18}_{-0.18}$	$+0.00^{+0.27}_{-0.27}$	$-0.10^{+0.38}_{-0.38}$	$-0.15^{+0.26}_{-0.26}$	$+0.05^{+0.27}_{-0.27}$	$-0.05^{+0.38}_{-0.38}$	$-0.30^{+0.45}_{-0.45}$	$-0.35^{+0.45}_{-0.45}$	–	–	–	–
12217324	$+0.22^{+0.14}_{-0.14}$	$+0.00^{+0.20}_{-0.20}$	$+0.30^{+0.15}_{-0.15}$	$-0.15^{+0.35}_{-0.35}$	$+0.10^{+0.35}_{-0.35}$	$+0.25^{+0.35}_{-0.35}$	$+0.55^{+0.35}_{-0.35}$	$-0.25^{+0.35}_{-0.35}$	$+0.15^{+0.44}_{-0.44}$	–	–	–	–	–

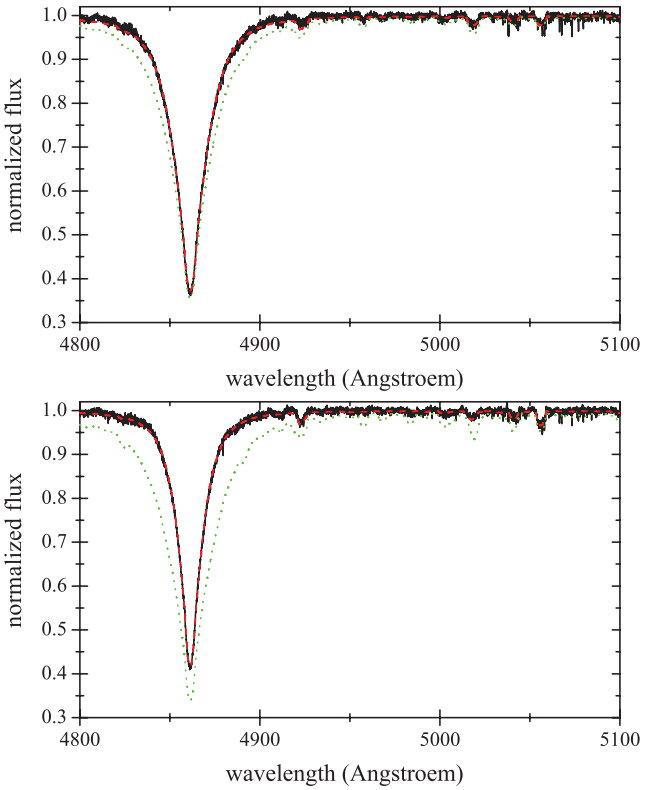

Figure 2. Fit of the observed (black, solid line) by synthetic spectra computed from our optimized parameters (red, dashed line) and from the values given in the KIC (green, dotted line). From top to bottom: KIC 02859567 and 03629496.

2MASS and Strömgren colours, accordingly. The first value agrees within the error bars with the one we determine spectroscopically in this study. The two spectra we obtained for KIC 10974032 are not enough to conclude about the presence of LPV. The light curve of this star is irregular, typical of that of an active star. The four spectra of KIC 08351193 do not show LPV either, though the star is classified as rotationally modulated by Balona et al. (2011).

KIC 02859567 and *03629496:* two fast rotating late B-type stars showing large deviations of the derived parameters from those listed in the KIC. Both stars show significant underabundances of Fe compared to the solar composition though consistent with the derived metallicity in both cases. Both show about solar He content and slight overabundances of Si. The spectrum of KIC 02859567 additionally exhibits an excess in Mg. Fig. 2 compares the observations with two synthetic spectra computed from our optimized and the KIC parameters in a small-wavelength region around H_β. The big difference in the quality of the fit is primarily explained by the difference in the assumed temperatures and confirms the conclusion made by Molenda-Zakowicz et al. (2010) that $T_{\rm eff}$ given in the KIC is too low for stars hotter than about 7000 K. The hotter the stars, the larger the deviation, in general. No signatures of binarity nor stellar activity could be found in the light curves of both stars. KIC 03629496 is classified by Balona (2011) as a beating star with a dominant contribution in the frequency range between 2 and 4 d^{-1} (23–46 μHz). KIC 02859567 in turn exhibits very low amplitude photometric variability in the same frequency regime making it an SPB candidate.

KIC 07974841 and *08018827:* both stars show clear variability in their light curves. KIC 07974841 is found in the Washington Double Star Catalog as WDS 19466+4346. The primary and secondary components are assumed to be of 8.24 and 11.32 mag, correspondingly; the magnitude of the primary is consistent with the visual magnitude found in the SIMBAD data base. The *Kepler* light curve of the star is too irregular to be explained by ellipsoidal effects occurring in close binary systems and is rather due to rotational modulation, stellar pulsations or a combination of both. Balona et al. (2011) classify the star as a rotationally modulated SPB variable, where the rotation signal dominates the pulsation one. Our two spectra do not show any variability that could be attributed to the binary nature of the star, neither global Doppler shifts of spectral lines nor any signature of the second star in the residuals of spectrum fitting. KIC 08018827 is reported by Balona et al. (2011) to be of B9 spectral type. Observed brightness variations are attributed to rotation effects. Fig. 3 shows a small portion of the *Kepler* light curve of this star. The light curve seems to be very regular showing both primary and secondary eclipses occurring every ∼0.4 d. The fact that the secondary eclipse occurs exactly at phase 0.5 relative to the primary minimum points towards a circular orbit which is expected for such close binary systems. Our two spectra are not enough to confirm binarity spectroscopically, however. The spectroscopically derived value of the effective temperature is right in between the two values reported by Balona et al. (2011) though closer to the one obtained from the SED fitting. Both stars are found to be much hotter than what is expected from the KIC. In both cases, we find that Fe and Si abundances are consistent with the derived metallicity while Mg is strongly enhanced for KIC 08018827 and slightly depleted for KIC 07974841. The latter star additionally exhibits strong depletion of He while nearly solar content of He is found for the former. Fig. 4 compares the Hβ line profile of KIC 07974841

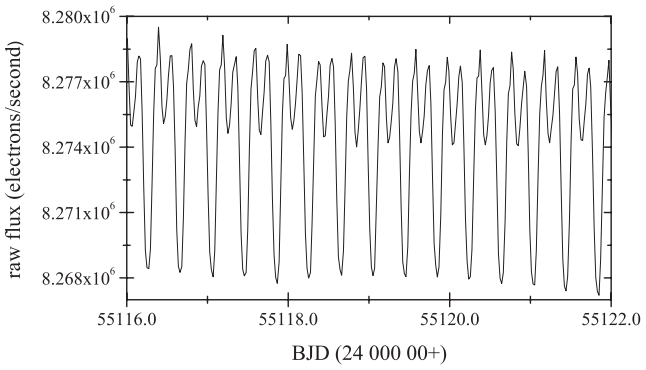

Figure 3. Part of the *Kepler* light curve of KIC 08018827.

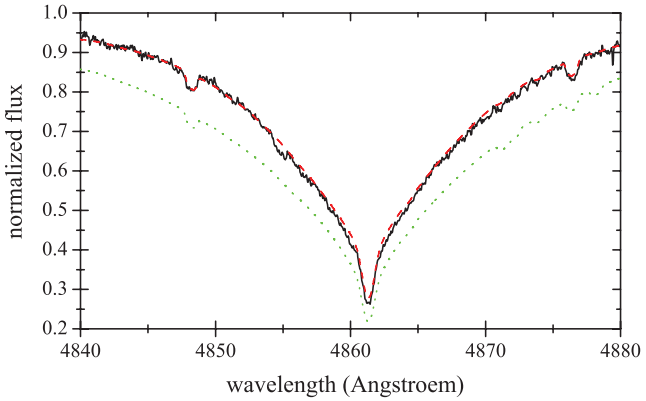

Figure 4. Same as Fig. 2 but for KIC 07974841.

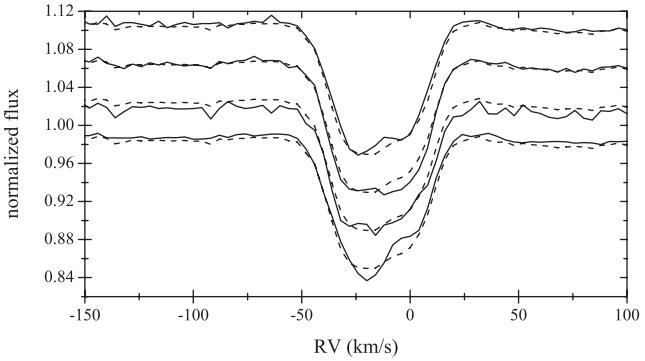

Figure 5. LSD profiles computed from four individual spectra of KIC 08324268. The average, dashed profile is given for comparison for better visibility of LPV.

(black, solid line) with the two synthetic profiles computed from our optimized parameters (red, dashed line) and from those listed in the KIC (green, dotted line). The difference is clearly visible showing that the KIC underestimates the temperature.

KIC 08324268: the star was classified as a chemically peculiar Si star by Zirin (1951) and is found in the Washington Double Star Catalog as WDS 19586+4416. Balona et al. (2011) report an effective temperature of about 14 400 ± 2000 K which is much higher than the temperature we derive in this work. From the light curve, the star seems to be a monoperiodic variable with a period of about 2 d, attributed by Balona et al. (2011) to rotational modulation due to stellar surface inhomogeneities. Our four spectra show clear variability caused by moving bumps across the line profiles. Fig. 5 shows these bumps in the least-squares deconvolved (LSD; Donati et al. 1997) profiles that are shifted in the *Y*-axis for clarity. Given that there is no signature of the second star in the spectra nor Doppler shifts of the spectral lines pointing to binarity, we can exclude binarity as a cause of the observed variability. The strong variability of KIC 08324268 does not allow us to obtain a reasonable fit of its mean spectrum. The derived fundamental parameters of the star are strongly affected by the variability and thus can be unreliable. Given that our fit of the mean observed spectrum is fairly bad, no individual abundances are available for this star.

KIC 12217324: this is the sharpest-lined object among all late B- to early A-type stars in our sample. The derived effective temperature is right in between the two values reported by Balona et al. (2011) and agrees with them within the error bars. Our fundamental parameters are also in good agreement with those listed in the KIC. The photometric variability of the star is attributed by Balona et al. (2011) to rotation effects. Our two spectra are not enough to confirm these findings spectroscopically. The star does not show any peculiarities in individual abundances except for a small depletion of Mg and O and a slight excess of Cr.

4.1.1 *Position in the* $\log(T_{\rm eff})-\log(g)$ *diagram*

In this section, we discuss the positions of the stars in the $\log(T_{\rm eff})-\log(g)$ diagram with respect to the theoretical SPB and β Cep instability strips as described by Miglio, Montalbán & Dupret (2007). Fig. 6 shows the position of the stars in the $\log(T_{\rm eff})-\log(g)$ diagram together with the theoretical SPB and β Cep instability strips, shown for two different values of metallicity – solar (dashed lines) and sub-solar (solid lines).

Table 4 summarizes the results of classification. According to their position in the $\log(T_{\rm eff})-\log(g)$ diagram, three of the hottest

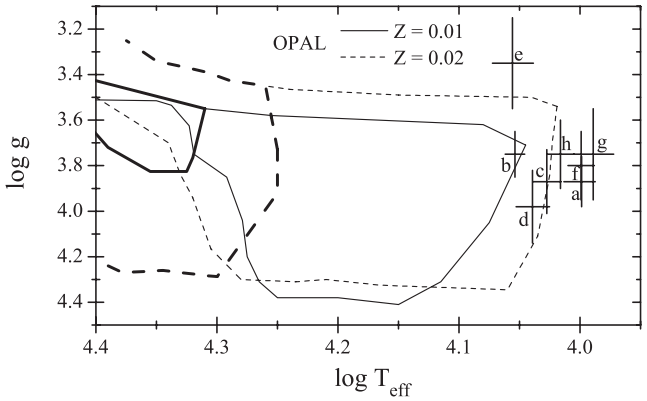

Figure 6. Location of the late B- to early A-type stars (see Table 4 for labels) and the SPB (thin lines) and β Cep (thick lines) theoretical instability strips in the $\log(T_{\rm eff})-\log(g)$ diagram. The instability regions are computed for two different metallicity values and are based on Miglio et al. (2007).

Table 4. Classification of late B- to early A-type stars based on their position in the $\log(T_{\rm eff})-\log(g)$ diagram.

KIC number	Variability		Label
	Diagram	Other	
03629496		Beating star (SPB?)[1]	b
07974841	SPBs	Rotation+SPB[2]	c
08018827		Rotation[2]/binary[3]	d
12217324	Possibly SPB	Rotation[2]	h
02859567		Possibly SPB[3]	a
08351193	Too cool	Rotation[2]	f
10974032		Rotation[3]	g
08324268	Too evolved	Rotation[2]	e

[1] Balona (2011), [2]Balona et al. (2011),
[3]This paper (light-curve morphology, visual inspection).

stars in our sample (labels b, c and d) are found to be SPB-type variables, one is classified as 'possibly SPB' (label h) and four stars are either too cool (labels a, f and g) or too evolved (label e) to be SPBs.

Two out of the four potential pulsators, KIC 08018827 and 12217324 (labels d and h), are claimed to be non-pulsating stars by Balona et al. (2011), who attribute their photometric variability to rotation effects. KIC 08018827 exhibits the light curve and Fourier spectrum typical of close binary systems. Binarity is expected to have an effect on the spectroscopically derived $T_{\rm eff}$ and $\log g$, and thus on the position of the star in the $\log(T_{\rm eff})-\log(g)$ diagram. This makes spectroscopic classification of this star rather uncertain. KIC 12217324 is found close to the cool edge of the SPB instability strip. Given that this star does not show remarkable LPV nor peculiarities in terms of individual abundances, it is considered by us as an SPB candidate pulsator.

Two out of three cool stars (labels f and g) are low-metallicity stars. Moreover, for both stars the light-curve morphology suggests rotational modulation due to stellar surface inhomogeneities. According to their position in the $\log(T_{\rm eff})-\log(g)$ diagram, these stars should not pulsate which confirms their photometric classification. KIC 02859567 (label a) is the only star among these three that shows low-amplitude SPB-type pulsations in its Fourier spectrum but is clearly outside the corresponding theoretical instability region.

According to its position in the diagram, KIC 08324268 (label e) is too evolved to be an SPB variable. However, the LPV detected

in the spectra of this star is so strong that it prevents the derivation of individual abundances and might affect the derived fundamental parameters. Thus, similar to KIC 08018827, the spectroscopic classification of this star is rather uncertain.

4.2 Intermediate A- to early F-type stars

In this section, we discuss a sub-sample of 18 γ Dor/δ Sct candidate stars. Twelve out of these 18 stars are divided into three arbitrary groups, 'stars with composite spectra', 'stars showing clear LPV' and 'stars with peculiar abundances', according to their type of spectrum variability. Finally, we classify the stars according to their positions in the $\log(T_{\rm eff})-\log(g)$ diagram and compare the results with the classification expected from the analysis of *Kepler* light curves.

4.2.1 Stars with composite spectra

KIC 04180199, 11572666 and *11874676:* three rapidly rotating stars exhibiting similar photometric and spectroscopic characteristics. The spectra are characterized by sharp central cores superimposed on the broad absorption features extending typically from -300 to $+300$ km s^{-1}. Fig. 7 (top) shows LSD profiles computed from nine individual spectra of KIC 04180199. The profiles are shifted in the *Y*-axis for clarity. The lines have broad wings and timely variable sharp central cores. The bottom panel of Fig. 7 compares the observed spectrum of KIC 04180199 with two synthetic spectra computed from our optimized parameters and convolved with different $v \sin i$ of 180 and 30 km s^{-1}. The positions of the majority of the spectral lines in the green spectrum coincide with the sharp features seen in the observed spectrum. The fact that both sharp and broad components are stationary in RV excludes binarity as a cause of the observed spectrum variability.

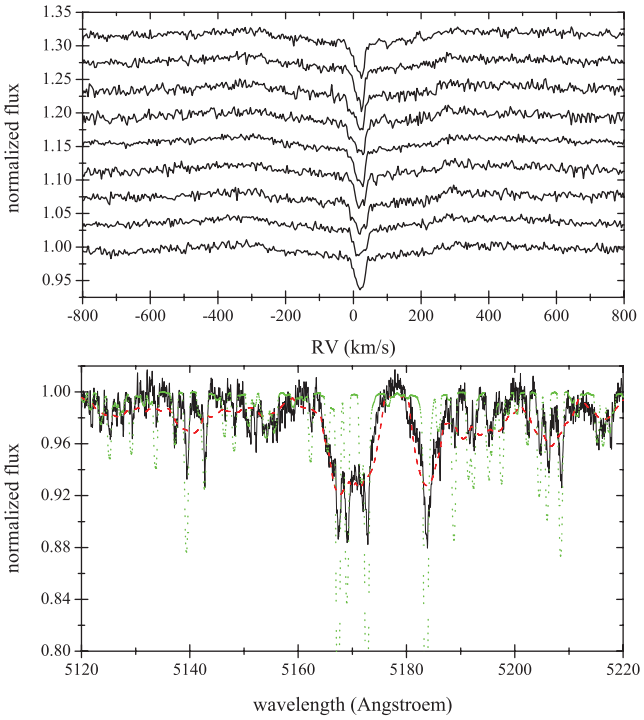

Figure 7. Top: LSD profiles computed from nine individual spectra of KIC 04180199. Bottom: fit of the observed (black, solid line) by the synthetic spectra computed from our optimized parameters and assuming $v \sin i$ of 180 km s^{-1} (red, dashed line) and 30 km s^{-1} (green, dotted line).

Mantegazza & Poretti (1996) report the detection of the composite spectrum of the δ Sct star X Caeli (HD 32846). Its spectral lines show a complex behaviour with sharp central cores superimposed on broad absorption features. The narrow core absorption was found to be stable in time both in shape and position, excluding stellar pulsations or orbital motion as first sight causes. Moreover, the RV of the core was found to be comparable to that of the stellar barycentre making it improbable that it comes from a foreground star, for example. The authors thus suggest a model consisting of a δ Sct variable star exhibiting broad spectral lines that has a circumstellar shell characterized by the narrow absorption cores superimposed on the photospheric lines of the central object. Our stars show a similar behaviour with the exception that the narrow absorption core seems to be variable on a short time-scale (cf. Fig. 7, top). None of the stars is referred as a binary in the literature. Instead, KIC 04180199 and 11572666 have been classified by Uytterhoeven et al. (2011) as hybrid γ Dor–δ Sct and KIC 11874676 as δ Sct pulsators.

All three stars have low metallicities with clear enrichment of Si, Mg and possibly C in their atmospheres. The difference between the derived and the KIC temperatures does not exceed 400 K in the worst case of KIC 11874676 while the deviations in $\log g$ are more remarkable and reach 0.6 dex in the case of KIC 11572666. Given the complexity of the spectra described above, both the fundamental parameters and the individual abundances are uncertain.

4.2.2 Stars showing clear LPV

KIC 02987660, 07304385, 09351622 and *10537907:* these are four stars showing remarkable LPVs in their spectra. Fig. 8 shows the individual LSD spectra of KIC 02987660 as an example of bumps moving across the profile, possibly caused by stellar oscillations. Two of the stars, KIC 02987660 and 07304385, are reported by Uytterhoeven et al. (2011) to be correspondingly δ Sct and γ Dor-type pulsators, while the two others, KIC 09351622 and 10537907, are found to be of γ Dor–δ Sct hybrid type. All four stars show individual abundances consistent with the derived metallicity within the errors of measurement.

4.2.3 Stars with peculiar abundances

KIC 05356349: though the star is in the Washington Double Star Catalog (WDS J19196+4035AB), Uytterhoeven et al. (2011)

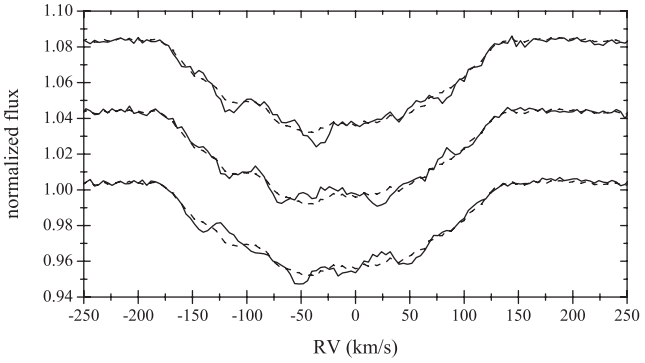

Figure 8. LSD profiles computed from three individual spectra of KIC 02987660. The average, dashed profile is given for comparison for better visibility of LPV.

classify it as a single star of γ Dor–δ Sct hybrid type. Our two spectra are not enough to conclude on binarity. Some peculiarities in individual abundances are detected, however. Ti and Cr are found to be underabundant by correspondingly 0.6 and 0.5 dex compared to the metallicity of the star, while Mg is enhanced by roughly the same value.

KIC 07827131: this star was first reported to be variable by Magalashvili & Kumsishvili (1976). It is classified as γ Dor–δ Sct hybrid pulsator by Uytterhoeven et al. (2011). According to our findings, this is a low-metallicity star with unusually low Ti content (-1.85 dex compared to the solar composition) and an enrichment of Si of about 0.6 dex compared to the derived metallicity. As for the previously discussed object, we have only two spectra which are not enough to conclude on either LPV or binarity.

KIC 08489712, 08915335 and *09291618:* these are three stars with an enhanced Si content, up to 0.9 dex compared to the derived metallicity in the case of KIC 08915335. According to Uytterhoeven et al. (2011), two stars, KIC 08489712 and 09291618, are pure γ Dor and δ Sct variables, accordingly, while the third star, KIC 08915335, has a light curve and Fourier spectrum characteristic of γ Dor–δ Sct-type hybrid pulsators. None of the three stars shows remarkable LPV nor Doppler shifts of spectral lines pointing to binarity.

4.2.4 *Position in the* $\log(T_{\rm eff})-\log(g)$ *diagram*

Fig. 9 shows the positions of all intermediate A- to early F-type stars of our sample in the $\log(T_{\rm eff})-\log(g)$ diagram, together with the δ Sct (solid lines) and γ Dor (dashed lines) observational instability strips as given by Rodríguez & Breger (2001) and Handler & Shobbrook (2002), accordingly.

Table 5 classifies the stars according to their type of variability, listing the classifications expected from their location in the $\log(T_{\rm eff})-\log(g)$ (Fig. 9) and derived by Uytterhoeven et al. (2011) from the frequency analysis of the *Kepler* light curves. We find three stars (labels m, v and z) which are too hot and five stars (l, n, q, r and s) which are too evolved to be γ Dor or δ Sct variables. Four of them, KIC 05356349, 07827131, 08489712 and 08915335 (labels m, q, r and s), exhibit peculiar individual abundances and have been discussed in detail in the previous section. KIC 12153021 (label z) does not show any remarkable variability in its light curve nor in the spectra and seems to be a constant star. Three further stars, KIC 04989900, 05437206 and 10096499 (labels l, n and v), have been found by Uytterhoeven et al. (2011) to show both γ Dor- and δ Sct-type pulsations; thus, they appear to be hotter from our spectroscopic analysis than what is expected from the photometric classification.

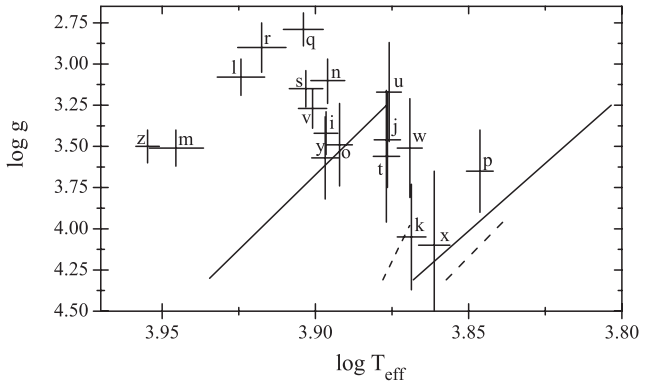

Figure 9. Location of intermediate A- to early F-type stars (see Table 5 for labels) and the γ Dor (dashed lines) and δ Sct (solid lines) observed instability strips in the $\log(T_{\rm eff})$–$\log(g)$ diagram.

Table 5. Classification of the intermediate A- to early F-type stars based on their position in the $\log(T_{\rm eff})-\log(g)$ diagram.

KIC number	Variability		Label
	Diagram	Other	
04180199	γ Dor or hybrid	Hybrid[1]	k
11572666			x
02987660	δ Sct	δ Sct[1]	j
09291618			t
07304385		γ Dor[1]	p
10537907			w
09351622	Possibly δ Sct	Hybrid[1]	u
02571868		δ Sct[1]	i
06668729			o
11874676			y
10096499		γ Dor[1]	v
05356349	Too hot	Hybrid[1]	m
12153021		Not pulsating[2]	z
04989900	Too evolved	Hybrid[1]	l
05437206			n
07827131			q
08915335			s
08489712		γ Dor[1]	r

[1] Uytterhoeven et al. (2011)
[2] This paper (light-curve morphology, visual inspection).

We confirm two γ Dor pulsators (labels k and x) and four δ Sct stars lying in the expected region of the $\log(T_{\rm eff})-\log(g)$ diagram. Three out of these six stars (labels k, x and w) have been classified by Uytterhoeven et al. (2011) as γ Dor–δ Sct hybrid pulsators, two stars (labels j and t) were reported as pure δ Sct variables and one (label p) as a γ Dor pulsator. Finally, four stars (labels i, o, u and y) are located close to the hot border of the δ Sct instability strip and are thus classified by us as 'possibly δ Sct' variables. At least one of these stars (label u) is expected to be of lower temperature from the theory of non-radial pulsations, however, as reported by Uytterhoeven et al. (2011) to show γ Dor-like oscillations in its light curve.

5 STELLAR TEMPERATURES FROM SEDS

The effective temperature of the stars can be estimated from the SED. For our target stars, the SED was constructed from literature photometry, using 2MASS (Sktrutskie et al. 2006), Tycho *B* and *V* magnitudes (Høg et al. 1997), USNO-B1 *R* magnitudes (Monet et al. 2003) and TASS *I* magnitudes (Droege, Richmond & Sallman 2006), supplemented with CMC14 *r′* magnitudes (Evans, Irwin & Helmer 2002) and TD-1 ultraviolet flux measurements (Carnochan 1979).

The SED can be significantly affected by interstellar reddening. We have, therefore, estimated this effect from the equivalent widths of the interstellar Na D lines present in our spectra. $E(B-V)$ was calculated using the relation given by Munari & Zwitter (1997). For resolved multicomponent interstellar Na D lines, the equivalent widths of the individual components were measured. The total $E(B-V)$ in these cases is the sum of the reddening per component, since interstellar reddening is additive (Munari & Zwitter 1997). The SED was de-reddened using the analytical extinction

Table 6. Stellar effective temperatures from SEDs.

KIC	$E(B-V)$	$T_{\rm eff}$	SED notes
02571868	0.01	8050 ± 330	TD-1
02859567	0.01	10070 ± 370	TD-1
02987660	0.01	7530 ± 300	TD-1
03629496	0.03	12130 ± 540	TD-1
04180199	0.08	7810 ± 370	CMC14 *r′*
04989900	0.06	8750 ± 230	TD-1
05356349	0.05	9150 ± 300	TD-1
05437206	0.04	7990 ± 320	TD-1
06668729	0.02	8120 ± 330	TD-1
07304385	0.06	7070 ± 320	
07827131	0.05	8580 ± 290	TD-1
07974841	0.07	10680 ± 420	TD-1
08018827	0.03	10240 ± 410	TD-1
08324268	0.05	10980 ± 520	TD-1
08351193	0.01	10760 ± 430	TD-1
08489712	0.08[a]	9020 ± 330	TD-1
08915335	0.14[a]	8600 ± 470	CMC14 *r′*
09291618	0.06	7760 ± 360	
09351622	0.06	7680 ± 340	
10096499	0.00	8370 ± 240	TD-1
10537907	0.06[a]	7500 ± 340	CMC14 *r′*
10974032	0.02	9380 ± 290	
11572666	0.07[a]	7260 ± 320	CMC14 *r′*
11874676	0.08	8300 ± 420	
12153021	0.01	8970 ± 310	TD-1
12217324	0.01	10360 ± 390	TD-1

[a]Indicates multicomponent interstellar Na D lines.

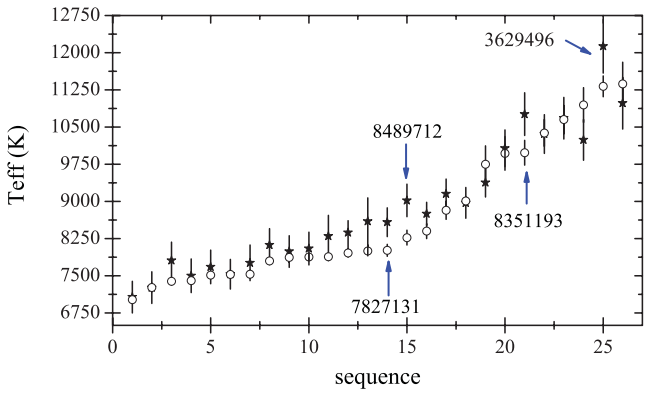

Figure 10. Comparison between the effective temperatures derived spectroscopically (open circles) and from the SED fitting (stars). The stars are sorted by the spectroscopic value starting with the coolest object.

fits of Seaton (1979) for the ultraviolet and Howarth (1983) for the optical and infrared.

The $T_{\rm eff}$ values were determined by fitting solar-composition Kurucz (1993) model fluxes to the de-reddened SED. For that, the model fluxes were convolved with photometric filter response functions. A weighted Levenberg–Marquardt non-linear least-squares fitting procedure was used to find the solution that minimized the difference between the observed and model fluxes. Since $\log g$ is poorly constrained by the SED, we fixed $\log g = 4.0$ for all the fits. The results are given in Table 6. The uncertainties in $T_{\rm eff}$ include the formal least-squares error and adopted uncertainties in $E(B-V)$ of ±0.02 and $\log g$ of ±0.5 added in quadrature.

Fig. 10 compares the spectroscopically derived effective temperatures with those obtained from the SED fitting. There are four stars (KIC 03629496, 07827131, 08351193 and 08489712) for which the difference between the two temperatures is larger than the quoted error bars, otherwise the values agree within the error of measurement. For all four stars, the SED temperatures are higher than the spectroscopic value. Two stars, KIC 07827131 and 08351193, are low-metallicity objects, both showing remarkable enhancement of Si abundance. This peculiarity can possibly explain the observed disagreement in temperatures. KIC 08489712 also shows a peculiar behaviour in the sense of significant over- and underabundances of Si and Ti, accordingly. There is no obvious reason why the two temperatures differ by about 800 K for KIC 03629496, however.

6 COMPARISON WITH THE KIC

Figs 11 and 12 compare the spectroscopically derived atmospheric parameters ($T_{\rm eff}$, $\log g$ and [M/H]) with the KIC values. The typical errors of the KIC data of ±200 K for $T_{\rm eff}$ and of ±0.5 dex for both $\log g$ and metallicity are assumed. As it was for the first time reported by Molenda-Zakowicz et al. (2010) and later on confirmed by Lehmann et al. (2011) that the KIC temperatures are systematically underestimated for stars hotter than about 7000 K. The same conclusion is valid for our stars: most of the stars from intermediate A to late B spectral type have spectroscopic temperatures remarkably higher than those listed in the KIC. The stars of later spectral types and thus of lower temperatures show good agreement with the KIC values within the errors of measurement. KIC 11874676 seems to be the only star which does not follow this general tendency as its spectroscopically derived $T_{\rm eff}$ value appears to be by about 350 K lower than that given in the KIC (cf. Fig. 11). We think that this deviation comes from the fact that KIC 11874676 has a composite spectrum which leads to wrong parameter values in our analysis.

Pinsonneault et al. (2012) published a revised temperature scale for long-cadence targets in the KIC. The authors derive effective temperatures based on *griz* filter photometry and compare their temperature scale to the published infrared flux method scale for $V_T JK_s$ (Casagrande et al. 2010). For field dwarfs, Pinsonneault et al. (2012) find a mean shift towards hotter temperatures relative to the KIC, of the order of 215 K, for both colour systems. Unfortunately, only one of our targets is included in the catalogue by Pinsonneault et al. (2012), and this and the seven of our targets included in Casagrande et al. (2010) have temperatures in the region where our values and the KIC values agree well.

The deviations between spectroscopic and KIC values in metallicity and (to some extent) surface gravity seem to be correlated with the parameter values itself. This is illustrated in Fig. 12 that shows the difference between ours and the KIC values versus the

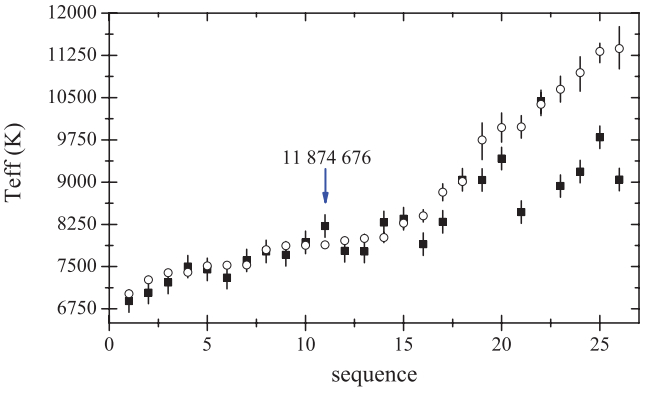

Figure 11. Same as Fig. 10 but for comparison with the KIC values (filled boxes).

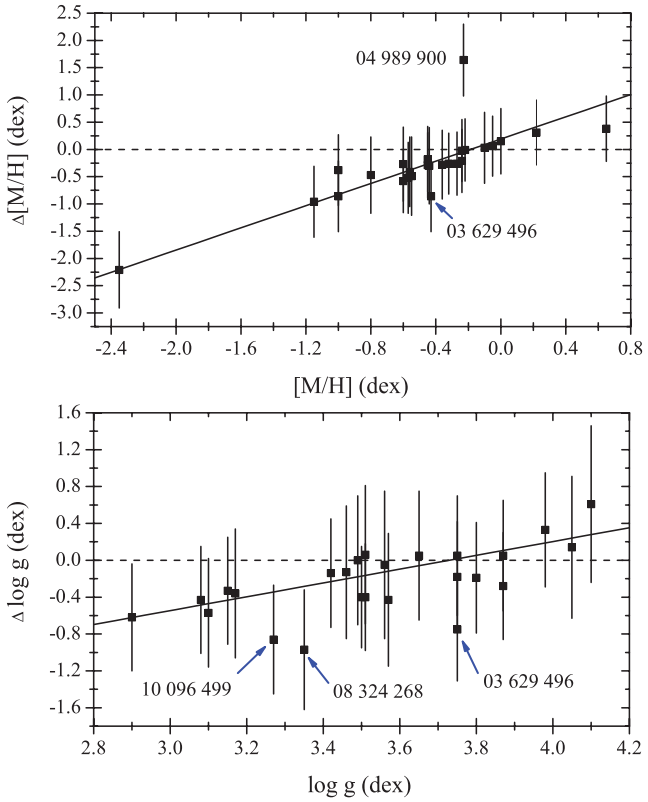

Figure 12. Comparison of the spectroscopically derived metallicity [M/H] (top) and surface gravity log *g* (bottom) with the KIC values. The solid lines represent linear fits to the data points after removing the marked outliers.

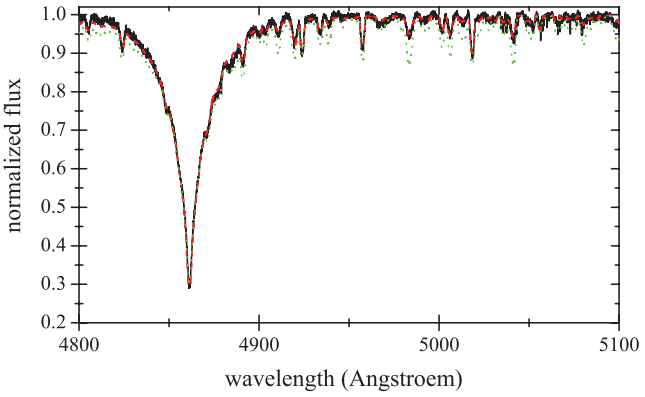

Figure 13. Fit of the observed spectrum of KIC 10096499 (black, solid line) by synthetic spectra computed from our optimized parameters (red, dashed line) and from the values given in the KIC (green, dotted line).

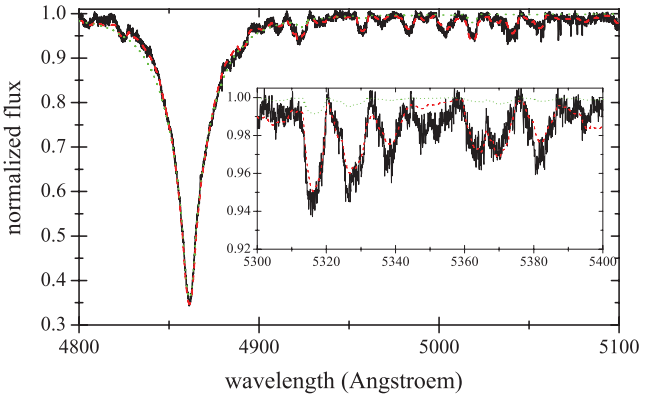

Figure 14. Same as Fig. 13 but for KIC 04989900.

spectroscopic values of the parameters. The given error bars are the combined spectroscopic and KIC errors. Stars that are outliers with respect to the observed general tendency are marked by their KIC numbers and discussed in the following.

KIC 03629496 and *08324268:* these are the two hottest stars in our sample both showing large discrepancy of more than 1500 K between spectroscopic and KIC temperatures. Thus, it is not surprising at all that they also show large deviations of the spectroscopically derived log *g* from the KIC values. KIC 03629496 additionally has larger Δ[M/H] than what would be expected from the observed general tendency for this parameter. In the case of KIC 08324268, neither our derived fundamental parameters nor the KIC values provide a satisfying fit of the observed spectrum, whereas our parameters are much more appropriate than the KIC ones for KIC 03629496 (cf. the bottom panel of Fig. 2 for the quality of the fit).

KIC 10096499: the deviation of the optimized log *g* from the KIC value is larger than what would be expected from the general tendency for this parameter. Our spectroscopic parameters provide a much better fit of the observations than the KIC values. Fig. 13 illustrates the quality of the spectrum fitted by two synthetic spectra computed from our optimized and KIC parameters.

KIC 04989900: this star is an obvious outlier in the [M/H]–Δ[M/H] plane. The KIC metallicity of −1.87 is much lower than our optimized value. Fig. 14 compares the observed (black, solid line) spectrum with two synthetic spectra computed from our optimized (red, dashed line) and the KIC (green, dotted line) fundamental parameters. It can be seen that the KIC-based fit seriously underestimates the strengths of the metal lines.

7 CONCLUSIONS

We used the spectral synthesis method to determine the fundamental atmospheric parameters of 26 stars in the *Kepler* satellite field of view, of which 18 were proposed to be γ Dor/δ Sct candidate pulsators (Uytterhoeven et al. 2011), and compare our values with those listed in the KIC. Similar to the results reported by Molenda-Zakowicz et al. (2010) and Lehmann et al. (2011), we find that the photometric KIC $T_{\rm eff}$ values are systematically underestimated for stars hotter than about 7000 K. Deviations that may reach several thousands kelvin for hot stars (see e.g. Lehmann et al. 2011) are probably due to the interstellar reddening that was not properly taken into account when estimating the KIC temperatures.

Comparing the spectroscopically derived values of [M/H] and log *g* with the KIC values, we find hints to a correlation of the deviations with the parameter values itself. The correlation is stronger for [M/H]. Four stars show larger deviations from this general tendency. Except for KIC 08324268 that shows strong LPV, our parameters provide a much better fit of the observed spectrum than the KIC values, however.

Comparison between the spectroscopically derived temperatures and those obtained from the SED fitting reveals good agreement for all but four stars. For three stars, KIC 07827131, 08351193 and 08489712, chemical composition peculiarities (particularly, Si and Ti abundances) might be a possible reason for the observed discrepancy.

The spectroscopically derived values of $T_{\rm eff}$ and $\log g$ allow us to place the stars in the $\log(T_{\rm eff})$–$\log(g)$ diagram and classify them by checking their location relative to the theoretical SPB/β Cep (for B-type stars) and observational γ Dor/δ Sct (for A- and F-type stars) instability strips. Our spectroscopic classification was then compared to the photometric one for B- (Balona 2011; Balona et al. 2011), A- and F-type (Uytterhoeven et al. 2011) stars. We confirm two SPB pulsators, KIC 03629496 and 07974841, and find two more stars, KIC 08018827 and 12217324, that fall into or lie close to the SPB instability region but were classified by Balona et al. (2011) as rotationally modulated stars. We detected a clear signature of eclipses in the light curve of KIC 08018827. Binarity can have an impact on the spectroscopically derived $T_{\rm eff}$ and $\log g$ which in turn biases the classification according to the type of variability. No such hints including LPV have been found for KIC 12217324. Three other stars, KIC 02859567, 08351193 and 10974032, are too cool to be SPBs and too hot to be δ Sct variables. According to the photometric classification, however, one of these stars (KIC 02859567) is possibly an SPB pulsator while the variability of two others is attributed to rotation effects. Finally, we find one star, KIC 08324268, which is too evolved to be an SPB pulsator but its spectroscopic parameters might be biased by strong LPV detected in the spectra.

Among the A–F type stars of our sample, we find two γ Dor pulsators (KIC 04180199 and 11572666) and four δ Sct stars lying in the expected region of the $\log(T_{\rm eff})-\log(g)$ diagram. Two out of these four stars show δ Sct oscillations in their light curves, in one star δ Sct and γ Dor-typical oscillations co-exist, and one star is a pure γ Dor pulsator. Four further stars, KIC 02571868, 06668729, 09351622 and 11874676, are located at the hot border of the δ Sct instability region. These stars are classified by us as 'possibly δ Sct' pulsators and one of them surprisingly shows γ Dor-typical oscillations in its light curves. Furthermore, we found eight stars that are either too hot or too evolved to be γ Dor- or δ Sct-type variables, though all but one show characteristic γ Dor-like pulsations in their light curves.

Uytterhoeven et al. (2011) present a general characterization of 750 candidate A–F type stars in the *Kepler* field of view and find strong evidence for the existence of γ Dor and δ Sct stars beyond the edges of the current observational instability strips. The authors conclude that a revision of the instability strips is needed in order to accommodate the *Kepler* δ Sct and γ Dor stars. The same conclusion is drawn by Grigahcène et al. (2010) concerning theoretical γ Dor and δ Sct instability strips. The authors characterize a sample of 234 stars showing δ Sct and γ Dor frequencies in their light curves and find that the borders of theoretical instability strips are not a good match for the observations. Similar to the findings of these two groups, we found that γ Dor-typical oscillations are much more common among the δ Sct stars than what is predicted by the corresponding instability strips and conclude that a revision of the latter is essential.

ACKNOWLEDGEMENTS

KU acknowledges financial support by the Spanish Ministry of Economy Competitiveness (MINECO) grant AYA2010-17803. The authors are grateful to the referee for very useful comments that led to significant improvement of the paper. This publication makes use of data products from the Two Micron All Sky Survey, which is a joint project of the University of Massachusetts and the Infrared Processing and Analysis Center/California Institute of Technology, funded by the National Aeronautics and Space Administration and the National Science Foundation. This research has made use of the SIMBAD data base, operated at CDS, Strasbourg, France.

REFERENCES

Aerts C., Christensen-Dalsgaard J., Kurtz D. W., 2010, Astronomy and Astrophysics Library, Asteroseismology. Springer, Berlin
Auvergne M. et al., 2009, A&A, 506, 411
Balona L. A., 2011, MNRAS, 415, 1691
Balona L. A. et al., 2011, MNRAS, 413, 2403
Carnochan D. J., 1979, Bull. Inf. Cent. Donnees Stellaires, 17, 78
Casagrande L., Ramírez I., Meléndez J., Bessell M., Asplund M., 2010, A&A, 512, A54
De Cat P., Daszyńska-Daszkiewicz J., Briquet M., Dupret M.-A., Scuflaire R., De Ridder J., Niemczura E., Aerts C., 2004, in Kurtz D. W., Pollard K. R. eds, IAU Colloq. 193: Variable Stars in the Local Group, Vol. 310. Astron. Soc. Pac., San Francisco, p. 195
Donati J.-F., Semel M., Carter B. D., Rees D. E., Collier Cameron A., 1997, MNRAS, 291, 658
Droege T. F., Richmond M. W., Sallman M., 2006, PASP, 118, 1666
Evans D. W., Irwin M. J., Helmer L., 2002, A&A, 395, 347
Fossati L., Bagnulo S., Monier R., Khan S. A., Kochukhov O., Landstreet J., Wade G., Weiss W., 2007, A&A, 476, 911
Fossati L., Bagnulo S., Landstreet J., Wade G., Kochukhov O., Monier R., Weiss W., Gebran M., 2008, A&A, 483, 891
Gilliland R. L. et al., 2010, PASP, 122, 131
Grevesse N., Asplund M., Sauval A. J., 2007, Space Sci. Rev., 130, 105
Grigahcène A. et al., 2010, ApJ, 713, L192
Handler G., Shobbrook R. R., 2002, MNRAS, 333, 251
Howarth I. D., 1983, MNRAS, 203, 301
Høg E. et al., 1997, A&A, 323, 57
Kaye A. B., Handler G., Krisciunas K., Poretti E., Zerbi F. M., 1999, PASP, 111, 840
Kupka F. G., Ryabchikova T. A., Piskunov N. E., Stempels H. C., Weiss W. W., 2000, Balt. Astron., 9, 590
Kurucz R. L., 1993, Kurucz CD-ROM 13. SAO, Cambridge, USA
Lehmann H. et al., 2011, A&A, 526, A124
Magalashvili N. L., Kumsishvili J. I., 1976, Inf. Bull. Var. Stars, 1167, 1
Mantegazza L., Poretti E., 1996, A&A, 312, 855
Miglio A., Montalbán J., Dupret M.-A., 2007, Commun. Asteroseismol., 151, 48
Molenda-Zakowicz J., Jerzykiewicz M., Frasca A., Catanzaro G., Kopacki G., Latham D. W., 2010, preprint (arXiv:1005.0985)
Molenda-Żakowicz J. et al., 2013, MNRAS, submitted
Monet D. G. et al., 2003, AJ, 125, 984
Munari U., Zwitter T., 1997, A&A, 318, 26
Pinsonneault M. H., An D., Molenda-Żakowicz J., Chaplin W. J., Metcalfe T. S., Bruntt H., 2012, ApJS, 199, 30
Rodríguez E., Breger M., 2001, A&A, 366, 178
Schmidt-Kaler Th., 1982, in Schaifers K., Voigt H. H., eds, Landolt-Börnstein, Vol. 2b. Springer-Verlag, Berlin
Seaton M. J., 1979, MNRAS, 187, 73
Shulyak D., Tsymbal V., Ryabchikova T., Stütz C., Weiss W. W., 2004, A&A, 428, 993
Skrutskie M. F. et al., 2006, AJ, 131, 1163
Tkachenko A., Lehmann H., Smalley B., Debosscher J., Aerts C., 2012, MNRAS, 422, 2960
Tsymbal V., 1996, in Adelman S. J., Kupka F., Weiss W. W., eds, ASP Conf. Ser. Vol. 108, M.A.S.S., Model Atmospheres and Spectrum Synthesis. Astron. Soc. Pac., San Francisco, p. 198
Uytterhoeven K. et al., 2010a, Astron. Nachr., 331, P30
Uytterhoeven K. et al., 2010b, Astron. Nachr., 331, 993
Uytterhoeven K. et al., 2011, A&A, 534, A125
Waelkens C., 1991, A&A, 246, 453
Zirin H., 1951, Harv. Coll. Obs. Bull., 920, 38

This paper has been typeset from a TEX/LATEX file prepared by the author.